$Sr_xTi_{1-x}CoO_{3\pm\delta}$ Perovskite-like Catalysts with Enhanced Activity for Hydrogen Production

Yan Liu[1], Huigu Li[1], Jia Huang[1], Xiaomin Hu[1], Yu Zhang[1], Prof. Dr. Lihong Huang[1,2]*
[1]Chengdu University of Technology, Department of Chemical and Pharmaceutical Engineering, Chengdu 610059, China
[2]Indiana University – Purdue University, Indianapolis, Richard G. Lugar Center for Renewable Energy, Indianapolis, IN 46202, USA
*Correspondence: Prof. Dr. Lihong Huang (E-mail: huanglihong06@cdut.cn), Chengdu University of Technology, Department of Chemical and Pharmaceutical Engineering, Chengdu 610059, China

Abstract

Auto-thermal reforming (ATR) of acetic acid (HAc) is a promising and alternative route for hydrogen production from renewable resources, while deactivation caused by cobalt metal sintering and coking is a major concern in ATR. In this paper, perovskite-like catalysts of $Sr_xTi_{1-x}CoO_{3\pm\delta}$(x=0, 0.2, 0.5, and 0.8) were prepared by evaporation induced self-assembly (EISA) method, and then evaluated in ATR for hydrogen production. The results showed that $Sr_xTi_{1-x}CoO_{3\pm\delta}$ catalysts exhibited optimized activity and stability: H_2 yield was recorded near 2.86 mol-H_2/mol-HAc with the conversion of HAc at 100%. Additionally, the Co particles with strong metal-support interaction of $SrTi(Co)O_3$ inhibited the formation of coking/ agglomeration, showing potential for hydrogen production via ATR process.
Keywords: Acetic acid, Auto-thermal reforming, Hydrogen production, Perovskite

1 Introduction

To address environmental issues caused by consumption of fossil fuels, hydrogen has been widely explored as an alternative and clean energy carrier [1, 2]. Bio-oil, which is produced via pyrolysis of biomass, is a feasible renewable resource for hydrogen production [3]; Acetic acid (HAc) is the main component of bio-oil with content up to 33.0%, and can be processed for hydrogen production through steam reforming[4], as listed in **Eq. 1**.

$$CH_3COOH + 2H_2O \rightarrow 2CO_2 + 4H_2 \quad \Delta H^0 = +131.4\ \text{kJ} \qquad (1)$$

$$CH_3COOH + 1.4H_2O + 0.28O_2 \rightarrow 2CO_2 + 3.44H_2 \quad \Delta H^0 = 0 \qquad (2)$$

Nevertheless, the strong endothermicity of steam reforming limits its practical operation and requires high quality steam resource to maintain the reforming process. Auto-thermal reforming (ATR) with oxygen in the feed stands out for its heat sustainability, as listed in **Eq. 2**[5, 6]. However, oxygen in the ATR feed is normally consumed in the leading upstream zone of the fixed-bed reactor with a high temperature (up to 1000°C), and deactivation by oxidation and sintering of catalysts can be found overtime[7] .

Received: June 18, 2021; revised: July 29, 2021; accepted: August 10, 2021

This is the author's manuscript of the article published in final edited form as:

Liu, Y., Li, H., Huang, J., Hu, X., Zhang, Y., & Huang, L. (2021). SrxTi1–xCoO3±δ Perovskite-like Catalysts with Enhanced Activity for Hydrogen Production. Chemical Engineering & Technology, 44(10), 1870-1876. https://doi.org/10.1002/ceat.202100285

Cobalt-based catalysts have been reported for their high activity and selectivity in ATR of HAc[4, 8]; however, deactivation caused by cobalt metal oxidation, sintering and coking[9] remains as the main concern for sustainable hydrogen production[10]. Accordingly, strategies on modification of crystal phases and strong metal-support interaction (SMSI) have been adopted[11], and specific structures, e.g., hydrotalcite-like structure, dolomite, olivine, solid solution and ordered mesoporous structure, were synthesized and presented improved reactivity, as reported in the previous work[12].

Perovskites, which are categorized as mixed oxides with a general formula of ABO_3, have attracted much attention for fabrication of improved catalysts [13], while ions within A-site or B-site can be partially or completely substituted by additives (Sr, Ca, Fe, etc.) to form perovskite-derived oxides[14, 15]; these oxides are capable of fabricating well-dispersed metallic particles, suppressing the formation of coke and increasing reactivity of catalysts. For example, as reported by Coelho et al.[16], a $CoTiO_3$ perovskite presented excellent activity in dry reforming of methane; however, the structure of perovskite was destroyed due to the reduction of Co species, resulting in the poor stability over time. In comparison, some other perovskites, such as $SrTiO_3$, are rather thermally stable to endure high temperatures [17]. Meanwhile, active metal of Co ions can be incorporated into the perovskite structure with a strong metal-support interaction, which can be then partially reduced to form surface active species in the reforming process[18].

In the current work, perovskite-like catalysts of $Sr_xTi_{1-x}CoO_{3\pm\delta}$(x=0, 0.2, 0.5, and 0.8) were prepared via evaporation induced self-assembly method, and tested in ATR process for hydrogen production. In addition, characterization techniques of XRD, N_2 physisorption, H_2-TPR, SEM and TG were carried out to explore active species, carriers and the relationship between the structure and catalytic performance.

2 Experimental

2.1 Catalyst preparation

The $Sr_xTi_{1-x}CoO_{3\pm\delta}$(x=0, 0.2, 0.5 and 0.8) catalysts were prepared by evaporation induced self-assembly (EISA) method. Chemicals of $Co(NO_3)_2{\cdot}6H_2O$ and $Sr(NO_3)_2$ were dissolved in deionized water; aqueous solution of $C_{16}H_{36}O_4Ti$ was diluted in hydrochloric acid (35% by volume), followed by addition of acetic anhydride; a triblock copolymer of P123 with a molar ratio of P123/(total molar of Co, Ti and/or Sr) = 0.01 was dissolved in anhydrous ethanol. Subsequently, the aforementioned solutions were mixed in a beaker, continuously stirred for 3h at 40°C, dried at 65°C for 48h, and calcined at 700°C in air atmosphere for 4h. The obtained $Sr_xTi_{1-x}CoO_{3\pm\delta}$ catalysts with different contents of Sr and Ti were denoted as TC-Sx (x=0, 0.2, 0.5 and 0.8), as listed in **Tab. 1**.

Table 1. List of $Sr_xTi_{1-x}CoO_{3\pm\delta}$ catalysts as prepared.

Catalysts	Molar compositions	S_{BET} of oxides [$m^2\ g^{-1}$]	Pore volume [$cm^3\ g^{-1}$]	Average pore size	Particle size of Co^0 estimated by XRD [a]	
					Reduced	Spent
TC-S0	$Ti_1Sr_0CoO_{3\pm\delta}$	8.2	0.04	5.7	29.8	29.5
TC-S0.2	$Ti_{0.8}Sr_{0.2}CoO_{3\pm\delta}$	16.1	0.12	19.9	23.4	23.6
TC-S0.5	$Ti_{0.5}Sr_{0.5}CoO_{3\pm\delta}$	10.0	0.05	10.1	16.5	16.6
TC-S0.8	$Ti_{0.2}Sr_{0.8}CoO_{3\pm\delta}$	7.2	0.03	7.0	27.9	---

[a] Estimated by the peak near 43.9° of the Co^0 phase.

2.2 Catalytic performance test

ATR of HAc was conducted in a quartz tubing fixed-bed reactor with an inner diameter of 4.0 mm. 200 mg of catalyst with grain size of 20~40 mesh was loaded and reduced in H_2 at 700°C for 1h. The pre-mixed feed of HAc and H_2O was introduced by a syringe pump (P230II, Elite Instrument), and vaporized at 280°C. The vapor was mixed with O_2 and N_2 at a molar ratio of $HAc/H_2O/O_2/N_2$=1:4:0.28:3.90, and then

introduced into the reactor at 11000 mL•g^{-1}•h^{-1}, 600°C and 1 atm. The products were analyzed online by a gas chromatography (GC-7890, Lunan Ruihong Instrument) equipped with TCD/FID detectors.

The selectivity of carbon-containing products (S_i), HAc conversion (X_{HAc}) and the hydrogen yield (Y_{H2}) were calculated by equations of (3), (4) and (5), respectively.

$$S_{i\ \text{carbon-containing product}} = \frac{F_{i\ \text{carbon-containing product}}}{n_i(F_{HAc\ in} - F_{HAc\ out})} \quad (3)$$

$$X_{HAc} = \frac{F_{HAc\ in} - F_{HAc\ out}}{F_{HAc\ in}} \quad (4)$$

$$Y_{H_2} = \frac{F_{H_2\ product}}{F_{HAc\ in}} \quad (5)$$

In the above equations, $F_{i,\ in\ or\ out}$ is the molar flow of i species at the inlet or the outlet of the reactor, and n_i represents the ratio of carbon between the carbon-containing products and HAc.

2.3 Characterizations

The X-ray diffraction (XRD) analysis was performed on an apparatus of DX-2700 (Haoyuan Instrument) with Cu K_α radiation (45 kV, 50 mA).

The specific surface areas, pore volumes and average pore diameters were determined by N_2 physisorption experiments at -196°C with an apparatus of JW-BK112, JWGB. Before each measurement, the catalysts were degassed at 300°C for 1 h.

The temperature-programmed reduction (TPR) experiments were carried out in a fixed-bed reactor with a TP-5076 device (Xianquan Instrument). 50 mg of the catalysts were pretreated at 300°C in N_2 for 1 h, and then cooled down to 30°C. The temperature increased linearly from 30°C to 900°C at a rate of 10°C/min in a 5.0 % H_2/N_2 flow.

The morphology of the catalysts was screened with a field emission scanning electron microscope (Quanta FEG, FEI, U.S.).

Thermogravimetric analysis was performed over an STA409 PC analyzer (NETZSCH, Germany). The catalysts were heated in flowing air from 30°C to 700°C at 10°C/min.

3 Results and discussion

3.1 Characterizations

3.1.1 Oxides of catalysts

To explore the crystal structures, the catalysts after calcination at 700°C were screened by XRD, as shown in **Fig. 1(A)**. Over the TC-S0 catalyst without Sr ($Ti_1Sr_0CoO_{3\pm\delta}$), strong diffraction peaks of rutile TiO_2 phase (PDF#21-1276) were discovered with trace of $CoTiO_3$ species (PDF#: 15-0866). With Sr partly replaced Ti in TC-S0.2 catalyst ($Ti_{0.8}Sr_{0.2}CoO_{3\pm\delta}$), the peaks of rutile TiO_2 phase weakened obviously and the peaks of $CoTiO_3$ disappeared, while trace of anatase TiO_2 phase (PDF#:21-1272) and perovskite of $SrTiO_3$ (PDF#: 35-0734) emerged.

With further substitution of Ti by Sr in TC-S0.5 catalyst($Ti_{0.5}Sr_{0.5}CoO_{3\pm\delta}$), there were only strong peaks of $SrTiO_3$ perovskite and no other phases were found, suggesting Co oxides could be highly dispersed and incorporated into the perovskite structure as $SrTi(Co)O_3$. For the TC-S0.8 catalyst($Ti_{0.2}Sr_{0.8}CoO_{3\pm\delta}$) with higher Sr content, the intensity of $SrTiO_3$ decreased, and species of $SrCoO_x$ (PDF#: 21-1307) were found; there were new peaks of Sr_2TiO_4 (PDF#: 39-1471), which belongs to the family of perovskite homologues in a general formula of A_2BO_4[19]. Besides, peaks of brookite TiO_2 (PDF#: 20-0011) emerged.

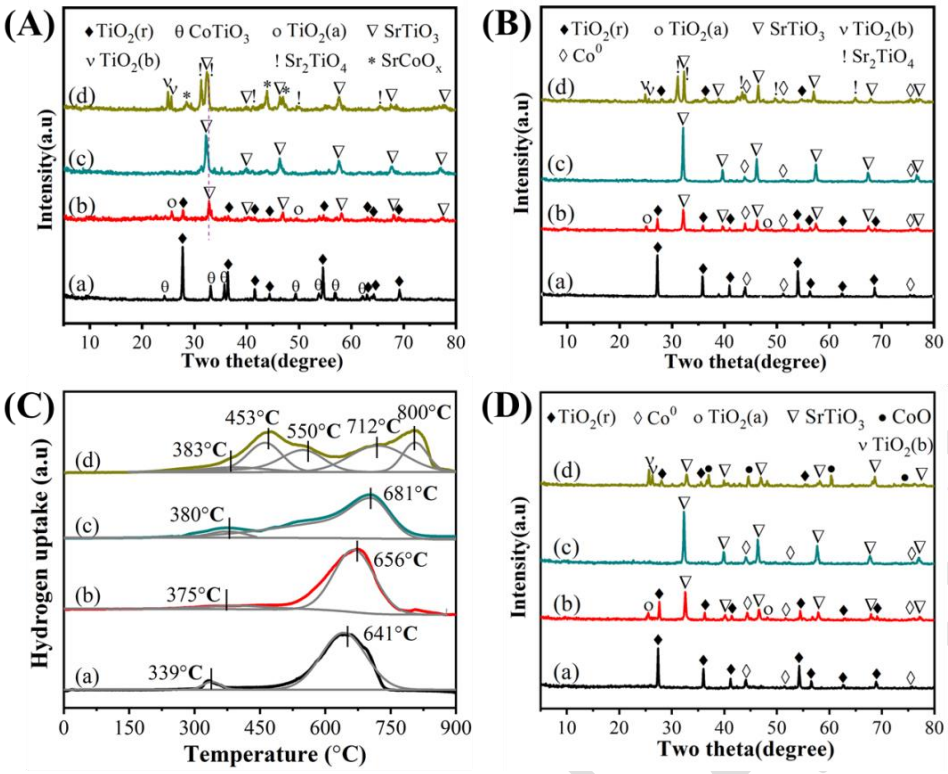

Figure 1. XRD patterns of (A) calcined catalysts, (B) reduced catalysts and (D) spent catalysts; H_2-TPR profiles (C) of catalysts: (a) TC-S0, (b) TC-S0.2, (c) TC-S0.5 and (d) TC-S0.8.

N_2 physisorption was used to evaluate the specific surface areas (S_{BET}), pore volume and average pore sizes of these catalysts, and the results were displayed in **Tab. 1** and **Fig. 2**. According to the IUPAC classification, the adsorption isotherm of TC-S0 catalyst can be categorized into Type III isotherm curve (typical for pore-free material). In comparison, the isotherms of TC-S0.2, TC-S0.5 and TC-S0.8 exhibited Type IV adsorption isotherm curve, corresponding to typical mesoporous materials. It can be seen from **Tab. 1** that there was a low S_{BET} of 8.2 m^2/g for the TC-S0 catalyst, which may be attributed to the main crystal phase of rutile TiO_2 with a low surface area[20]. With Ti partly replaced by Sr, the S_{BET} reached 16.1 m^2/g in TC-S0.2, but declined with more Sr in TC-S0.5 and TC-S0.8.

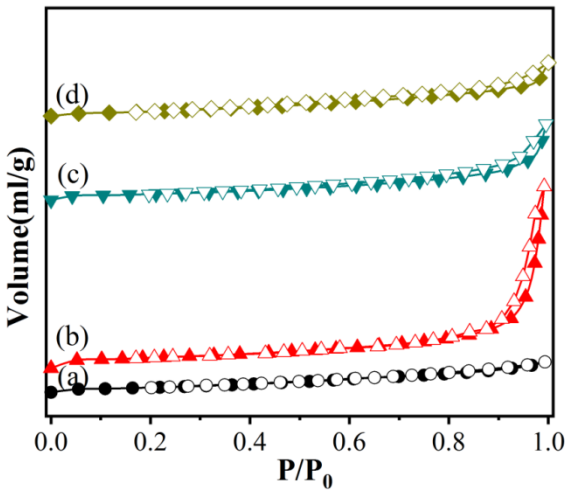

Figure 2. Nitrogen adsorption/desorption isotherms of calcined catalysts: (a) TC-S0, (b) TC-S0.2, (c) TC-S0.5 and (d) TC-S0.8.

SEM images were collected to explore the surface morphology of the calcined catalysts, as shown in **Fig. 3**. Relatively small particles were found in TC-S0.2, which is consistent with the high surface area at 16.1 m^2/g from BET analysis. For TC-S0.8 catalyst, the particles are larger, which can be attributed to the decrease of specific surface area.

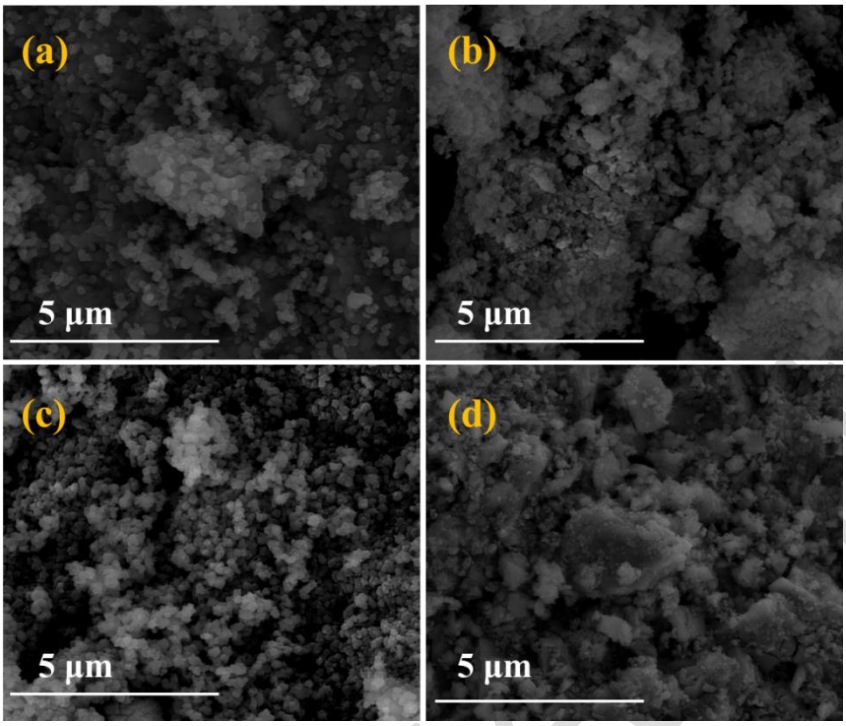

Figure 3. SEM images of calcined catalysts: (a) TC-S0, (b) TC-S0.2, (c) TC-S0.5 and (d) TC-S0.8.

3.1.2 Reduced catalysts

After reduction in hydrogen for 1h, the catalysts were screened with XRD, as presented in **Fig. 1(B)**. For the TC-S0 catalyst, the perovskite-type oxides of $CoTiO_3$ were completely collapsed and transformed to cobalt metal (Co^0)(JCPDS#:15-0806) and rutile TiO_2 via reaction of $CoTiO_3 + H_2 \rightarrow Co^0 + TiO_2 + H_2O$ [16]. Over the TC-S0.2 catalyst, the perovskite-type oxides of $SrTiO_3$ and TiO_2 phase still remained; meanwhile, the weak peaks of Co^0 emerged. For the TC-S0.5 catalyst, the single perovskite structure of $SrTiO_3$ were stable during the reduction process, and the peaks of Co^0 were observed, which can be caused by the reduction of highly dispersed cobalt oxide within the perovskite-like $SrTi(Co)O_3$ structure, as suggested by XRD. For the TC-S0.8 catalyst, the peaks of brookite TiO_2 weakened, while the peaks of $SrCoO_x$ transformed to cobalt metal species.

The particle size was calculated by Scherrer equation based on the Co(111) diffraction peak at 43.9°, as listed in **Tab. 1**. The Co^0 particle size was calculated to be 29.8nm, 23.4 nm, 16.5 nm and 27.9 nm over TC-S0, TC-S0.2, TC-S0.5 and TC-S0.8, respectively. Noticeably, the TC-S0.5 catalyst showed the smallest particles size of Co^0 among these catalysts, indicating the perovskite structure of $SrTi(Co)O_3$ could prevent the agglomeration of Co particles and stabilize cobalt particles during the reduction process[21].

H_2-TPR experiments were performed to study the redox properties of TC-Sx catalysts, as shown in **Fig. 1(C)**. For the TC-S0 catalyst, a weak reduction peak near 339°C belongs to the reduction of amorphous species of CoO_x, and a main peak near 641°C is attributed to the reduction of $CoTiO_3$ species[22]. With Sr partly replaced Ti in TC-S0.2 catalyst, similar reduction peaks of amorphous species of CoO_x were found, a main peak near 656°C can be assigned to the reduction of cobalt species within the $SrTi(Co)O_3$ perovskite structure. Two similar reduction peaks of Co species were found in the TC-S0.5 catalyst; however, the

higher temperature reduction peak of $SrTi(Co)O_3$ shifted to 681°C, suggesting there were enhanced interactions between Co species and mixed oxide support within $SrTi(Co)O_3$. With more Sr in TC-S0.8 catalyst, peaks near 435°C and 550°C could be attributed to the reduction of $SrCoO_x$ in two steps, namely Co^{3+} to Co^{2+} and Co^{2+} to Co^0, respectively. Besides, the reduction peak at 800°C can be assigned to Ti species within the Sr_2TiO_4 structure.

3.2 Catalytic performance of the $Sr_xTi_{1-x}CoO_{3\pm\delta}$ catalysts

3.2.1 Reactivity in ATR of HAc

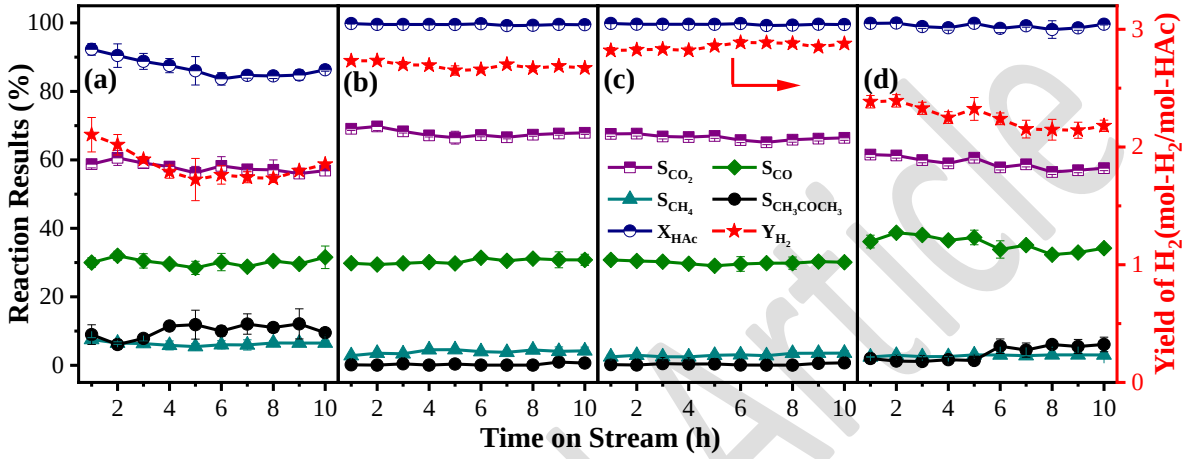

Figure 4. Catalytic performance of $Sr_xTi_{1-x}CoO_{3\pm\delta}$ catalysts in ATR of HAc at 11000 ml$\cdot g^{-1}\cdot h^{-1}$, 600°C and 1 atm: (a) TC-S0, (b) TC-S0.2, (c) TC-S0.5 and (d) TC-S0.8.

To evaluate reactivity of these Co-based catalysts, auto-thermal reforming of HAc was conducted for hydrogen production at 600°C firstly, and the average values and standard deviations were calculated based on two parallel experiments. As shown in **Fig. 4(a)**, for the TC-S0 catalyst without Sr, the HAc conversion started near 92% and then dropped continuously to 84.7% in the end; meanwhile, the H_2 yield declined from 2.10 mol-H_2/mol-HAc to 1.79 mol-H_2/mol-HAc. For the carbon-containing products, the selectivities to CO_2 and CO was around 59.1% and 30.5%, respectively. In addition, the selectivity to by-products of CH_4 and CH_3COCH_3 was recorded at 6.5% and 12.1%, respectively, suggesting that more HAc were transformed via ketonization route. Over the TC-S0.2 catalyst with Sr in **Fig. 4(b)**, the HAc conversion maintained near 100% and the H_2 yield was stable near 2.69 mol-H_2/mol-HAc.

For the TC-S0.5 catalyst with more Sr **(Fig. 4(c))**, a better catalytic performance was observed: the HAc conversion was kept at 100% and H_2 yield were stable near 2.86 mol-H_2/mol-HAc. The increase in the H_2 yield can be explained by the variation of carbon-containing products: the selectivity to CO_2 remained about 65.8%, the selectivity to CO slightly decreased to near 29.4%; meanwhile, only trace of CH_4 was detected and CH_3COCH_3 disappeared, indicating that the ketonization pathway was constrained. For the TC-S0.8 catalyst with higher Sr content in **Fig. 4(d)**, the H_2 yield declined from 2.38 to 2.14 mol-H_2/mol-HAc. Meanwhile, the selectivity of CH_3COCH_3 increased to 6.1%, suggesting that HAc was partly converted into acetone via ketonization route.

3.2.2 Catalytic performance of catalysts with different O_2/HAc and temperatures

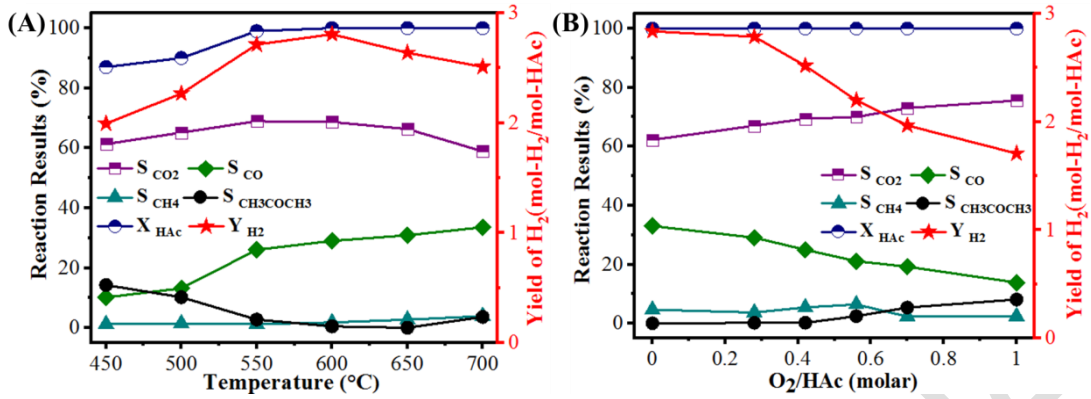

Figure 5. Effect of (A) temperatures and (B) O_2/HAc on the catalytic performance over TC-S0.5 in ATR of HAc.

The TC-S0.5 performed better at 600°C in ATR of HAc, and was then further tested with different temperatures and ratios of O_2/HAc. As shown in **Fig. 5(A)** with different temperatures, at 450°C, the HAc conversion started at about 87.1 %, and the H_2 yield was around 1.99 mol-H_2/mol-HAc, which was due to the high selectivity to acetone near 14.3%. With increasing temperature, the HAc conversion increased to 100%, while the H_2 yield increased gradually to 2.81 mol-H_2/mol-HAc; meanwhile, acetone was not detected at 600°C. For a higher temperature at 700°C, the H_2 yield dropped slightly to 2.51 mol-H_2/mol-HAc because of the increased CO selectivity via the reverse water gas shift reaction (RWGSR) ($CO_2+H_2 \rightarrow CO+H_2O$). The results suggest that 600°C is the optimal temperature for ATR of HAc.

For the effect of O_2/HAc in **Fig. 5(B)**, the HAc conversion was stable around 100%, and the H_2 yield near 2.83 mol-H_2/mol-HAc was recorded at O_2/HAc=0. With oxygen in feeding at O_2/HAc=0.28 for ATR of HAc, the hydrogen yield was about 2.79 mol-H_2/mol-HAc. With higher O_2/HAc up to 1, the H_2 yield gradually decreased to 1.70 mol-H_2/mol-HAc, while selectivity to CO_2 increased and selectivity to CO dropped gradually, which was due to oxidation of hydrogen and increase of CO_2/CO. Considering the thermal balance and the hydrogen yield in ATR, the ratio of O_2/HAc near 0.28 can be accepted for ATR in the current work.

3.3 Spent catalysts

To find variations on structures of these Co-based catalysts during ATR process, the spent catalysts after the 10-h ATR reaction were screened with XRD, as presented in **Fig. 1(D)**. For the spent TC-S0 catalyst, the peaks of Co^0 species and rutile TiO_2 still remained. For the spent catalysts of TC-S0.2 and TC-S0.5, the perovskite-type oxides of $SrTiO_3$ and Co^0 species also remained stable and no obvious variation in particle size of Co^0 was found, suggesting that the $SrTiO_3$ skeleton was stable within the ATR atmosphere. In comparison, within the spent TC-S0.8 catalyst, the peaks of $SrTiO_3$ species became weaker and the peaks of Sr_2TiO_4 disappeared; meanwhile, peaks of CoO and rutile TiO_2 emerged, suggesting that the Co-$SrTiO_3$/Sr_2TiO_4 in TC-S0.8 have transformed into separate species of CoO, SrO and TiO_2, which means oxidation of Co^0 occurred and could result in deactivation during ATR process.

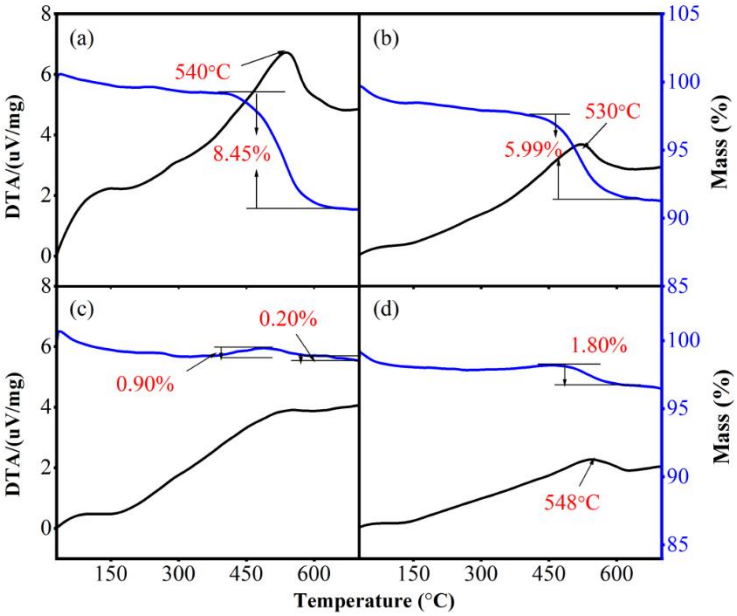

Figure 6. TG/DTA patterns of spent catalysts: (a) TC-S0, (b) TC-S0.2, (c) TC-S0.5 and (d) TC-S0.8.

Coking can be another reason for deactivation, and to find possible coking during ATR, TG-DTA analysis was performed over these spent catalysts, as shown in **Fig. 6**. The weight loss below 200°C can be attributed to the evaporation of water, while the weight loss at 500-600°C was assigned to the gradual combustion of carbonous species(Gao et al. 2018; Yang et al. 2010; Yu et al. 2012). The weight loss of coke over spent catalysts varied in a sequence as followed: TC-S0.5(0.20%) <TC-S0.8(1.80%) <TC-S0.2 (5.99%) <TC-S0 (8.45%). Among these catalysts, the TC-S0 catalyst without Sr presented a high weight loss than the other three samples; meanwhile, a stronger exothermic peak at 558.0°C was found in DTA (**Fig. 6(a)**), which can be attributed to combustion of carbon deposition. While for TC-S0.5 catalyst with Sr, no obvious carbon species was found, and a weight gain peak emerged near 400°C with an exothermic peak, which can be attributed to oxidation of cobalt metal. The weight gain peak of oxidation of cobalt metal was also checked by TG/DTA analysis on fresh reduced TC-S0.5 catalysts, and a weight gain peak with exothermic peak near 400 °C was found as well, confirming that oxidation of cobalt metal happened during the TG/DTA process.

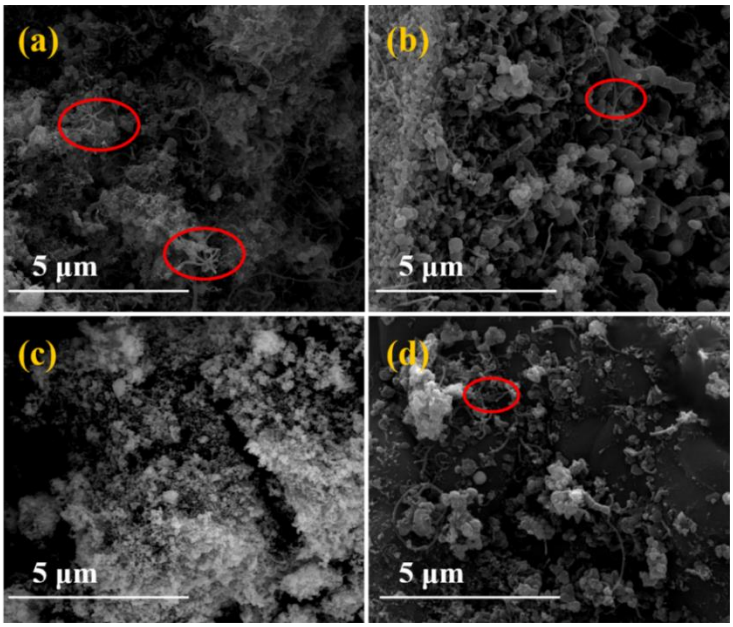

Figure 7. SEM images of spent catalysts: (a) TC-S0, (b) TC-S0.2, (c) TC-S0.5 and (d) TC-S0.8.

The SEM images of spent catalysts were also recorded, as shown in **Fig. 7**. For the TC-S0 catalyst, obvious filamentous carbon species were found over the catalyst surface, which was in consistent with the weight loss peak of coke in TG-DTA. No obvious carbon species was found over the TC-S0.5 catalyst. For the TC-S0.2 and TC-S0.8 catalyst, trace carbon species were observed.

3.4 Discussion

Based on the results of characterizations, for the TC-S0 catalyst without Sr, rutile TiO_2 was the main phase with trace of $CoTiO_3$ perovskite species. A low S_{BET} was measured at 8.2 m^2/g with an average pore size near 5.7 nm, which can be attributed to the main crystal phase of rutile TiO_2 with few crystal defects, as indicated by XRD and N_2 physisorption. After reduction, $CoTiO_3$ species transformed to TiO_2 and Co metal with a large particle size of 29.8 nm. Therefore, the TC-S0 catalyst showed a low activity: the HAc conversion started near 92% in the beginning, and then dropped continuously to 83.4%; meanwhile, the H_2 yield started near 2.13 mol-H_2/mol-HAc, but declined to 1.68 mol-H_2/mol-HAc. In the meantime, the selectivities to by-products of CH_3COCH_3 and CH_4 were high near 20.8% and 3.5%, respectively. Over the spent TC-S0 catalyst, coking was observed, explaining the HAc conversion gradually decreased over time.

For the TC-S0.5 catalyst with Ti partly replaced by Sr, a perovskite structure of $SrTiO_3$ was formed as the main phase; meanwhile, the Co species was highly dispersed within the $SrTiO_3$ skeleton with a strong interaction, forming a $SrTi(Co)O_3$ structure, as suggested by XRD and TPR. After reduction, Co metal with a particle size near 16.5 nm was obtained. The TC-S0.5 catalyst presented excellent activity and stability: the HAc conversion remained near 100%, H_2 yield were stable near 2.86 mol-H_2/mol-HAc. Over the spent catalysts, results of XRD, SEM and TG/DTA indicate that there was neither sintering nor coking during ATR, suggesting that the stable perovskite structure of $SrTiO_3$ with small Co particles was capable to resist the high temperature in ATR. Over the TC-S0.5 catalyst, partial replacement of Ti by Sr increased the surface defect sites and lattice defect structure of the perovskite catalyst. The introduction of SrO improved the alkalinity of the support surface, which was conducive to the adsorption and diffusion of the reactants CH_3COOH, H_2O and O_2, and then activated to form CH_3COO*, OH* and O* species, CH_3COO* was further decomposed into CH_3CO* at the active site, inhibiting intermediate products such as ketene, thereby suppressed the formation of carbon deposition.

For the TC-S0.8 catalyst with more Sr content, $SrTiO_3$ species decreased, and another perovskite structure of Sr_2TiO_4 existed as the main phase with trace of brookite TiO_2 and $SrCoO_x$. After reduction, Co metal with particle size near 27.9 nm was obtained via reduction of $SrCoO_x$ species and surface amorphous of CoO species. However, during the ATR test, the perovskite structure of Sr_2TiO_4 was destroyed and partly

transformed into separate species of SrO and TiO_2. Furthermore, trace of coke was found as well. As a result, deactivation over the TC-S0.8 catalyst was found with the H_2 yield decreased to 1.99 mol-H_2/mol-HAc overtime.

4 Conclusions

The perovskite-type oxides of $Sr_xTi_{1-x}CoO_{3\pm\delta}$ were prepared by evaporation induced self-assembly method and tested in ATR of HAc. Fine Co metallic particles and strong metal-support interaction were observed within the TC-S0.5 catalyst which derived from perovskite-type $SrTiO_3$ oxides, forming a stable $SrTi(Co)O_3$ structure. Therefore, the TC-S0.5 catalyst presented excellent activity and stability: the HAc conversion remained near 100%, and H_2 yield stable near 2.86 mol-H_2/mol-HAc. Besides, neither coking nor sintering was found, suggesting that the stable perovskite structure of $SrTi(Co)O_3$ with small Co particles and strong interaction inhibited agglomeration in ATR process, showing potential for hydrogen production via ATR of HAc.

Acknowledgements

The current work was financially supported by International Cooperation Program from Sichuan Science and Technology Program (2019YFH0181) and National Natural Science Foundation of China (21506111).

Declarations

Conflict of interest: On behalf of all authors, the corresponding author states that there is no conflict of interest.

Abbreviations

ATR		Auto-thermal reforming
EISA		Evaporation induced self-assembly
S_i	%	Selectivity
SEM		Scanning electron microscope
TG		Thermogravimetric
TPR		Temperature-programmed reduction
X_{Hac}	%	HAc conversion
XRD		X-ray diffraction
Y_{H2}	mol-H_2/mol-Hac	Hydrogen yield

References

[1] S. Al-Zuhair, M. Hassan, M. Djama, A. Khaleel, *Chem. Eng. Commun*. **2017**, *204*, 141-148. doi: 10.1080/00986445.2016.1245186

[2] S. Moogi, I. G. Lee, K. R. Hwang, *Int. J. Hydrogen Energy*. **2020**, *45*, 28462-28475

[3] F. Lai, E. Miao, L. Zuo, H. Lu, Y. Huang, T. Liu, *Small*. **2016**, *12*, 3235-3244. doi:10.1002/smll.201600412

[4] H. Li, X. Jia, N. Wang, B. Chen, X. Xie, Q. Wang, L. Huang, *Appl. Catal. B-Environ*. **2019**, *267*, 118730. doi:10.1016/j.apcatb.2019.118370

[5] W. Xie, J. Yang, Q. Wang, L. Huang, N. Wang, *Catal. Sci. Technol*. **2018**, *8*, 3015-3024. doi:10.1039/c8cy00116b

[6] A. Arandia, A. Remiro, V. Garcia, P. Castano, J. Bilbao, A. G. Gayubo, *Catalysts*. **2018**, *8*, 25. doi:10.3390/catal8080322

[7] L. Huang, Q. Liu, R. Chen, A. T. Hsu, *Appl. Catal. A-Gen*. **2011**, *393*, 302-308. doi:https://doi.org/10.1016/j.apcata.2010.12.010

[8] A. Kumar, R. Singh, A. S. K. Sinha, *Int. J. Hydrogen Energy*. **2019**, *44*, 12983-13010. doi:https://doi.org/10.1016/j.ijhydene.2019.03.136

[9] M. Dan, M. Mihet, M. D. Lazar, *Int. J. Hydrogen Energy*. **2020**, *45*, 26254-26264

[10] D. L. Li, S. P. Xu, K. Song, C. Q. Chen, Y. Y. Zhan, L. L. Jiang, *Appl. Catal. A-Gen*. **2018**, *552*, 21-29. doi:10.1016/j.apcata.2017.12.022

[11] J. P. d. S. Q. Menezes, K. R. Duarte, M. M. V. M. Souza, *Catal. Lett*. **2021**, *151*, 980-992. doi:10.1007/s10562-020-03366-x

[12] M. S. Feng, J. D. Liu, F. B. Zhang, L. H. Huang, *Chem. Pap*. **2015**, *69*, 1166-1175

[13] S. Dama, S. R. Ghodke, R. Bobade, H. R. Gurav, S. Chilukuri, *Appl. Catal. B-Environ*. **2018**, *224*, 146-158. doi:https://doi.org/10.1016/j.apcatb.2017.10.048

[14] K. Zhao, F. He, Z. Huang, G. Wei, A. Zheng, H. Li, Z. Zhao, *Appl. Energy*. **2016**, *168*, 193-203. doi:https://doi.org/10.1016/j.apenergy.2016.01.052

[15] A. Jahangiri, H. Aghabozorg, H. Pahlavanzadeh, *Int. J. Hydrogen Energy*. **2013**, *38*, 10407-10416. doi:https://doi.org/10.1016/j.ijhydene.2013.05.080

[16] D. C. Coelho, A. C. Oliveira, J. M. Filho, A. C. Oliveira, A. F. Lucredio, E. M. Assaf, E. Rodríguez-Castellón, *Chem. Eng. J*. **2016**, *290*, 438-453. doi:https://doi.org/10.1016/j.cej.2016.01.051

[17] S. I. Suárez-Vázquez, S. Gil, J. M. García-Vargas, A. Cruz-López, A. Giroir-Fendler, *Appl. Catal. B-Environ*. **2018**, *223*, 201-208. doi:https://doi.org/10.1016/j.apcatb.2017.04.042

[18] L. Zhao, T. Han, H. Wang, L. Zhang, Y. Liu, *Appl. Catal. B-Environ*. **2016**, *187*, 19-29. doi:https://doi.org/10.1016/j.apcatb.2016.01.007

[19] Y. S. Jia, S. Shen, D. G. Wang, X. Wang, J. Y. Shi, F. X. Zhang, H. X. Han, C. Li, *J. Mater. Chem. A* **2013**, *1*, 7905-7912. doi:10.1039/c3ta11326d

[20] M. T. Colomer, A. Del Campo, *J. Mater. Sci*. **2019**, *54*, 9414-9425. doi:10.1007/s10853-019-03550-4

[21] S. M. De Lima, A. M. Da Silva, L. O. O. Da Costa, J. M. Assaf, G. Jacobs, B. H. Davis, L. V. Mattos, F. B. Noronha, *Appl. Catal. A-Gen*. **2010**, *377*, 181-190. doi:https://doi.org/10.1016/j.apcata.2010.01.036

[22] O. U. Osazuwa, C. K. Cheng, *J. Clean. Prod*. **2017**, *148*, 202-211. doi:https://doi.org/10.1016/j.jclepro.2017.01.177

Table and Figure captions

Table 1. List of $Sr_xTi_{1-x}CoO_{3\pm\delta}$ catalysts as prepared.

Figure 1. XRD patterns of (A) calcined catalysts, (B) reduced catalysts and (D) spent catalysts; H_2-TPR profiles (C) of catalysts: (a) TC-S0, (b) TC-S0.2, (c) TC-S0.5 and (d) TC-S0.8.

Figure 2. Nitrogen adsorption/desorption isotherms of calcined catalysts: (a) TC-S0, (b) TC-S0.2, (c) TC-S0.5 and (d) TC-S0.8.

Figure 3. SEM images of calcined catalysts: (a) TC-S0, (b) TC-S0.2, (c) TC-S0.5 and (d) TC-S0.8.

Figure 4. Catalytic performance of catalysts in ATR of HAc at 11000 $ml \cdot g^{-1} \cdot h^{-1}$, 600°C and 1 atm: (a) TC-S0, (b) TC-S0.2, (c) TC-S0.5 and (d) TC-S0.8.

Figure 5. Effect of (A) temperatures and (B) O_2/HAc on the catalytic performance over TC-S0.5 in ATR of HAc.

Figure 6. TG/DTA patterns of spent catalysts: (a) TC-S0, (b) TC-S0.2, (c) TC-S0.5 and (d) TC-S0.8.

Figure 7. SEM images of spent catalysts: (a) TC-S0, (b) TC-S0.2, (c) TC-S0.5 and (d) TC-S0.8.

Table of Contents

Perovskite-like catalysts of $Sr_xTi_{1-x}CoO_{3\pm\delta}$ were prepared by EISA, Co species was incorporated into perovskite to form a stable $SrTi(Co)O_3$ structure, the perovskite-like $SrTi(Co)O_3$ catalyst showed excellent activity in ATR of HAc, the strong metal-support interaction suppressed carbon deposition and sintering.